Available online at www.sciencedirect.com
ScienceDirect
Journal of Computational Physics 227 (2008) 6351–6371
JOURNAL OF COMPUTATIONAL PHYSICS
www.elsevier.com/locate/jcp

A hybrid method to study flow-induced deformation of three-dimensional capsules

Y. Sui [a], Y.T. Chew [a], P. Roy [b], H.T. Low [b,*]

[a] Department of Mechanical Engineering, National University of Singapore, 9 Engineering Drive 1, Singapore 117576, Singapore
[b] Division of Bioengineering, National University of Singapore, 9 Engineering Drive 1, Singapore 117576, Singapore

Received 30 October 2007; received in revised form 3 March 2008; accepted 10 March 2008
Available online 18 March 2008

Abstract

A hybrid method is proposed to study the transient deformation of liquid filled capsules with elastic membranes under flow. In this method, the immersed boundary concept is introduced into the framework of lattice Boltzmann method, and the multi-block strategy is employed to refine the mesh near the capsule to increase the accuracy and efficiency of computation. A finite element model is incorporated to obtain the forces acting on the membrane nodes of the three-dimensional capsule which is discretized into flat triangular elements. The present method was validated by studying the transient deformation of initially spherical and oblate-spheroidal capsules with various membrane constitutive laws under shear flow; and there were good agreements with previous theory or numerical results. The versatility of the present method was demonstrated by studying the effects of inertia on the deformation of capsules in shear flow; and the inertia effects were found to be significant. The transient deformation of capsules with initially biconcave discoid shape in shear flow was also studied. The unsteady tank-treading motion was observed, in which the capsule undergoes periodic shape deformation and inclination oscillation while its membrane is rotating around the liquid inside. To our knowledge, this motion of three-dimensional biconcave discoid capsules has not been fully recovered by numerical simulation so far.

Keywords: Three-dimensional capsule deformation; Fluid–structure interaction; Multi-block lattice Boltzmann method; Immersed boundary method; Finite element model

1. Introduction

The flow-induced deformation of a liquid filled capsule enclosed by a thin elastic membrane has been studied by many researchers in cellular biology, bioengineering and chemical engineering. It is important in fundamental research as well as in biomedical and industrial applications. Furthermore it is the first step to model more complex flow situations which involve capsule suspensions, such as human microcirculation, cell filtration and drug delivery.

* Corresponding author. Tel.: +65 6516 2225; fax: +65 6779 1459.
E-mail address: mpelowht@nus.edu.sg (H.T. Low).

0021-9991/$ - see front matter © 2008 Elsevier Inc. All rights reserved.
doi:10.1016/j.jcp.2008.03.017

In the dynamic motion of capsules under flow, the fluid–structure interaction plays a key role. The complex mechanism of fluid–structure interaction makes theoretical analysis quite difficult. In most theoretical studies [1,2], simple geometry and small deformation of the capsules are assumed. As an alternative approach, numerical simulation has attracted much attention.

The arbitrary Lagrangian Eulerian (ALE) method [3,4] is a direct strategy to treat fluid–structure interaction. The boundary of the fluid domain moves with the motion of the fluid–structure interface, and the mesh is reconstructed. The ALE method has high-order accuracy but is very computationally expensive. For capsules with complex geometry or under large deformation, the re-meshing procedure will be very difficult and time-consuming.

The advected-field method, directly inspired by the phase-field approach, was proposed by Biben and Misbah [5]. The local membrane incompressibility is imposed to the phase-field approach, and the shear elasticity of the membrane is not taken into account. The advected-field method is suitable to deal with the deformation of vesicles, which are liquid drops enclosed by incompressible membranes. However, vesicles are different from capsules which are liquid drops enclosed by elastic membranes.

The boundary element method (BEM) [6] is most prevailing for studying capsule deformation in Stokes flow. One significant advantage of BEM is that the governing equations are solved only on the capsule interface, and thus the geometrical dimension of the problem can be reduced by one. With BEM, Pozrikidis and coworkers [7–9] and Lac et al. [10] have studied the transient deformation of capsules with various shapes and membrane properties, and obtained results consistent with experiments. The BEM is valid for creeping flow conditions. For capsules with complex shapes, like the biconcave disk, the simulation of tank treading motion was of limited duration because of numerical instabilities due to grid degradation [8].

The immersed boundary method (IBM) was developed by Peskin [11,12], to simulate blood flow in the heart. In this method, a force density is distributed to the Cartesian mesh in the vicinity of the moving boundary in order to account for the its effect. The force density is calculated from the boundary's constitutive law. With IBM, Eggleton and Popel [13] studied the large deformation of three-dimensional capsules in shear flow. However, the capsule response was followed for short times due to heavy computational load.

The lattice Boltzmann method (LBM), a kinetic based approach for simulating fluid flow, has been developed extensively and proven to be a robust and efficient method for solving complex fluid systems [14–17]. The standard lattice Boltzmann method, which employs a uniform Cartesian mesh, has been combined with immersed boundary method by Feng and Michaelides [18,19] for solving rigid particles flow. Recently, Lallemand et al. [20] coupled the lattice Boltzmann method with the front tracking method to study the dynamics of deformable interface with surface tension. Filippova et al. [21], as well as Yu and Girimaji [22] have proposed the multi-block lattice Boltzmann method, in which the computational domain is divided into blocks: fine mesh covers the blocks in which the gradients are large and coarse mesh is employed for other blocks. The computational efficiency of lattice Boltzmann method has been substantially improved by the multi-block strategy.

Recently, Peng et al. [23] applied the multi-block strategy in the immersed boundary lattice Boltzmann method (IB-LBM), and studied flow past two-dimensional stationary solid boundaries. The present authors [24,25] also combined these methods and studied the transient behaviors of two-dimensional capsules which deform under flow. Two-dimensional simulation shares a number of common features with three-dimensional study. However, it must be noted that for flow-induced deformation of capsules, two-dimensional simulation is a large simplification. Furthermore, the numerical modeling capsules in two and three dimensions are very different. Three-dimensional numerical modeling is much more complicated. For example, the membrane of a two-dimensional capsule is an elastic ring, and it is not difficult to discretized it into a set of line elements. The membrane tension can also be easily obtained from the strain of the line elements. For three-dimensional capsules, the discretization of the membrane involves plane elements, and the approach to obtain the membrane tension is not so straightforward as that of two-dimensional study.

In the present paper, the IB-LBM with multi-block strategy [24] is extended to three-dimensional simulation. The capsule membrane is discretized into unstructured flat triangular elements. To obtain the forces acting on the membrane nodes, a finite element model [26,27] is incorporated into the multi-block IB-LBM.

The flow field is solved by LBM, and the capsule interface is explicitly tracked by IBM. Only the computational domain near the capsule is covered by fine mesh, so that the computational accuracy and efficiency is

increased. The present method is validated by studying the transient deformation of initially spherical and oblate spheroidal capsules with various membrane constitutive laws under shear flow. The versatility of the present method is demonstrated by studying the effects of inertia on the deformation of capsules, and the deformation of capsules with complex shape like the biconcave discoid.

2. Membrane model

Three different membrane laws are tested. The three-dimensional capsule is discretized into flat triangular elements. The forces acting on the membrane nodes are obtained from a finite element model.

2.1. Membrane constitutive laws

In the present study, three different membrane constitutive laws are employed and tested. The capsule membranes are usually relatively thin, and thus the thickness can be neglected. A simple constitutive equation is the neo-Hookean (NH) law, with strain energy function having the form:

$$W^{\mathrm{NH}} = \frac{1}{6}E\left(I_1 - 1 + \frac{1}{I_2 + 1}\right) \tag{1}$$

where E is the surface shear elasticity modulus, and I_1 and I_2 are the first and second strain invariants, with $I_1 = \lambda_1^2 + \lambda_2^2 - 2$, $I_2 = (\lambda_1\lambda_2)^2 - 1$. The term λ_1 and λ_2 are the principle strains. The NH law corresponds to membranes made of polymerized material. The area dilation is unrestricted and is compensated by the thinning of the membrane.

The zero-thickness (ZT) shell equation is another version of the neo-Hookean (NH) law, which has been used by Ramanujan and Pozrikidis [8]:

$$W^{\mathrm{ZT}} = \frac{1}{6}E\left[I_1 - \log(I_2 + 1) + \frac{1}{2}\log^2(I_2 + 1)\right] \tag{2}$$

The two strain energy functions (Eqs. (1) and (2)) are equivalent for small deformation.

Another constitutive equation is the Skalak's law (SK) proposed by Skalak et al. [28] to model the membrane of red blood cells:

$$W^{\mathrm{SK}} = \frac{1}{4}E\left(\frac{1}{2}I_1^2 + I_1 - I_2\right) + \frac{1}{8}CEI_2^2 \tag{3}$$

In the right hand side of the equation, the first term represents the shear effects, and second term accounts for the area dilation. The term C is the ratio between shear elasticity modulus and area dilation modulus, which is quite large for incompressible biological membranes.

2.2. Membrane disretization

The 3D capsule membrane is discretized into flat triangular elements. The triangulation procedure is similar to that of Ramanujan and Pozrikidis [8]. To discretize the unstressed interface, each triangular face of a regular octahedron is subdivided into 4^n triangular elements. These elements are then projected radically onto a sphere. The geometry of each element is described by its three vertices. The discretization of a sphere surface is shown in Fig. 1(a). For oblate spheroid with aspect ratio b/a, the mapping system is stated as

$$x_{\mathrm{obl}} = Rx, y_{\mathrm{obl}} = Ry, z_{\mathrm{obl}} = (b/a)Rz \tag{4}$$

For the biconcave discoid, which is chosen to be the shape of red blood cell at rest, the mapping system is as follows:

$$x_{\mathrm{rbc}} = Rx, \quad y_{\mathrm{rbc}} = Ry, \quad z_{\mathrm{rbc}} = 0.5R(1 - r^2)^{0.5}(0.207 + 2.003r^2 - 1.123r^4) \tag{5}$$

where $r^2 = x^2 + z^2$, the term R in Eqs. (4) and (5) is the adjusting factor to keep the capsule volume constant. The discretization of a biconcave discoid surface is shown in Fig. 1(b).

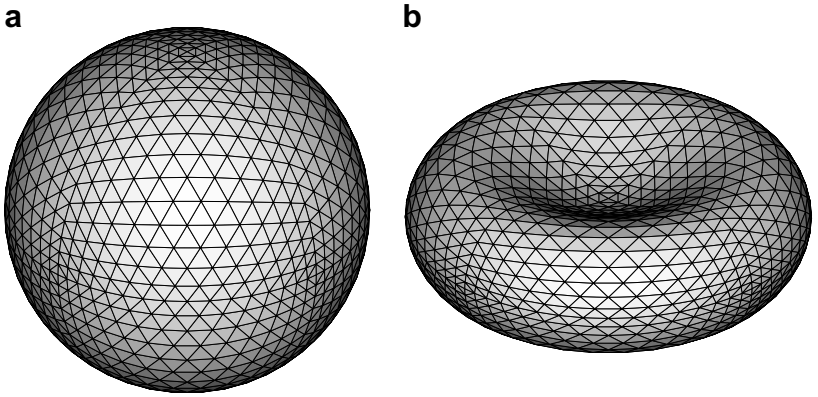

Fig. 1. Discretization of (a) a sphere; (b) a biconcave disk shape.

2.3. Finite element membrane model

A finite element membrane model is employed to obtain the forces acting at the discrete nodes of the membrane. In this section, only a brief description of this model is given. The detailed treatment can be found in Charrier [26] as well as Shrivastava and Tang [27].

In the finite element model, the membrane of the capsule is represented by a patchwork of flat triangular elements which remain flat after deformation, and the load on a element is represented by concentrated loads on the membrane nodes. Only in-plane stresses and strains exist. In the three-dimensional deformation of the capsule, the membrane elements do not stay in the same plane after being displaced. In this model, the deformed element is transformed to the plane of the undeformed element, so that the relative displacement of the nodes and the corresponding forces are easily determined. The equations developed for the force exerted at the nodes of an element of the deformed membrane are given in the plane of the element.

The displacements are approximated by linear shape functions in the plane of the element with coordinates (x', y'). They are described by: $\chi(x', y') = ax' + by' + c$. The unknown coefficients a, b, and c are determined using known values of the displacements at the three nodes of the element. After the displacements of the three nodes of an element are known, its state of strain λ_1 and λ_2 can be obtained. The relation of membrane strain and membrane energy is governed by the constitutive law, which is determined by the membrane materials. With a constitutive law chosen, one can follow the usual finite element procedure and derive the relations between nodal forces and nodal displacements. The principle of virtual work is used to calculate the forces at the three nodes of an element. Because each node of the discrete membrane belongs to more than one element, the resultant force on a node is the sum of the forces exerted by the m elements attached to the node. So far, the force calculated is the fluid force acting on the capsule membrane. Its equal and opposite counterpart is the force acting on the fluid. It is distributed to the surrounding fluid by the approach described by the immersed boundary method.

3. Numerical method

In the present hybrid approach, several methods are combined to simulate the flow-induced deformation of three-dimensional capsules. The immersed boundary concept is introduced into the framework of lattice Boltzmann method. The multi-block strategy is employed to refine the mesh near the capsule to increase the accuracy and efficiency of computation. The finite element membrane model, described in the previous section, is incorporated to obtain the membrane forces of the immersed boundary method.

3.1. Immersed boundary method

In the immersed boundary method of Peskin [11,12], a force density is distributed to the Cartesian mesh in the vicinity of the moving boundary in order to account for the effect of the boundary. To explain the

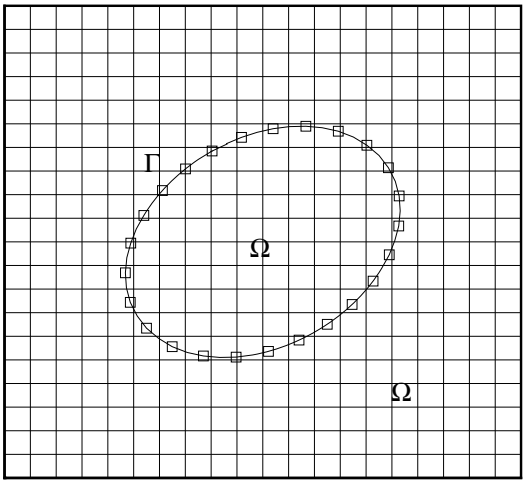

Fig. 2. Schematic illustration of a body whose boundary has been divided into Lagrangian nodes immersed in a Cartesian mesh.

immersed boundary method, consider a massless elastic capsule with boundary Γ immersed in the fluid domain Ω (see Fig. 2). The fluid domain Ω is represented by Eulerian coordinates $\mathbf{x}$, while the boundary of the capsule Γ, is represented by Lagrangian coordinates $\mathbf{s}$. Any position on the capsule membrane can be written as $\mathbf{X}(\mathbf{s},t)$. The term $\mathbf{F}(\mathbf{s},t)$ represents the membrane force density induced by capsule deformation, and the term $\mathbf{f}(\mathbf{x},t)$ represents the fluid body force density.

The non-slip boundary condition is satisfied by letting the flexible membrane move at the same velocity as the fluid around it. That is

$$\frac{\partial \mathbf{X}(\mathbf{s},t)}{\partial t} = \mathbf{u}(\mathbf{X}(\mathbf{s},t),t) \tag{6}$$

This motion will cause the capsule to deform. The membrane force density $\mathbf{F}(\mathbf{s},t)$ is obtained from the finite element membrane model discussed in Section 2.3, and is distributed to the fluid mesh points near it by

$$\mathbf{f}(\mathbf{x},t) = \int_{\Gamma} \mathbf{F}(\mathbf{s},t)\delta(\mathbf{x}-\mathbf{X}(\mathbf{s},t))\mathrm{d}\mathbf{s} \tag{7}$$

where δ is a smoothed approximation of the Dirac Delta function. In the present three-dimensional study, it is chosen to be:

$$\delta(\mathbf{x}-\mathbf{X}(\mathbf{s},t)) = \delta(x-X(\mathbf{s},t))\delta(y-Y(\mathbf{s},t))\delta(z-Z(\mathbf{s},t)) \tag{8}$$

where

$$\delta(r) = \begin{cases} \frac{1}{4}\left(1+\cos\left(\frac{\pi|r|}{2}\right)\right) & r \leqslant 2 \\ 0 & r > 2 \end{cases} \tag{9}$$

The same approximation function is used to obtain the velocities of the Lagrangian nodes on the moving boundary. The mathematical form can be written as follows, which illustrates the implementation of Eq. (6):

$$\frac{\partial \mathbf{X}}{\partial t} = \int_{\Omega} \mathbf{u}(\mathbf{x},t)\delta(\mathbf{x}-\mathbf{X}(\mathbf{s},t))\mathrm{d}\mathbf{x} \tag{10}$$

3.2. Multi-block lattice Boltzmann method

The lattice Boltzmann method is a kinetic-based approach for simulating fluid flows. It decomposes the continuous fluid flow into pockets of fluid particles which can only stay at rest or move to one of the neighboring

nodes. The D3Q19 model (see Fig. 3) is one of the commonly used models in 3D simulation, in which the discrete lattice Boltzmann equation has the form of [29]:

$$f_i(\mathbf{x}+\mathbf{e}_i\Delta t, t+\Delta t) - f_i(\mathbf{x},t) = -\frac{1}{\tau}[f_i(\mathbf{x},t) - f_i^{\mathrm{eq}}(\mathbf{x},t)] \tag{11}$$

where $f_i(\mathbf{x},t)$ is the distribution function for particles with velocity $\mathbf{e}_i$ at position $\mathbf{x}$ and time t, Δt is the lattice time interval, $f_i^{\mathrm{eq}}(\mathbf{x},t)$ is the equilibrium distribution function and τ is the non-dimensional relaxation time.

In the D3Q19 model, the fluid particles have the possible discrete velocities stated as follows:

$$\begin{aligned}&[\mathbf{e}_0,\mathbf{e}_1,\mathbf{e}_2,\mathbf{e}_3,\mathbf{e}_4,\mathbf{e}_5,\mathbf{e}_6,\mathbf{e}_7,\mathbf{e}_8,\mathbf{e}_9,\mathbf{e}_{10},\mathbf{e}_{11},\mathbf{e}_{12},\mathbf{e}_{13},\mathbf{e}_{14},\mathbf{e}_{15},\mathbf{e}_{16},\mathbf{e}_{17},\mathbf{e}_{18}]\\ &= \begin{bmatrix} 0 & 1 & -1 & 0 & 0 & 0 & 0 & 1 & 1 & -1 & -1 & 1 & -1 & 1 & -1 & 0 & 0 & 0 & 0 \\ 0 & 0 & 0 & 1 & -1 & 0 & 0 & 1 & -1 & 1 & -1 & 0 & 0 & 0 & 0 & 1 & 1 & -1 & -1 \\ 0 & 0 & 0 & 0 & 0 & 1 & -1 & 0 & 0 & 0 & 0 & 1 & 1 & -1 & -1 & 1 & -1 & 1 & -1 \end{bmatrix}\end{aligned} \tag{12}$$

The equilibrium distribution function $f_i^{\mathrm{eq}}(\mathbf{x},t)$ is in the form of:

$$f_i^{\mathrm{eq}} = E_i(\rho,\mathbf{u}) \tag{13}$$

$$\text{with } E_i(\rho,\mathbf{u}) = \omega_i\rho\left[1+\frac{\mathbf{e}\cdot\mathbf{u}}{c_s^2}+\frac{\mathbf{uu}:(\mathbf{e}_i\mathbf{e}_i - c_s^2\mathbf{I})}{2c_s^4}\right] \tag{14}$$

where ω_i is the weighing factor, it equals 1/3 for $i=0$, 1/18 for $i=1$–6 and 1/36 for $i=7$–18. The term c_s represents the sound speed, and equals $\Delta x/(\sqrt{3}\Delta t)$.

The relaxation time is related to the kinematic viscosity in Navier–Stokes equation in the form of

$$\nu = \left(\tau - \frac{1}{2}\right)c_s^2\Delta t \tag{15}$$

Once the particle density distribution is known, the fluid density and momentum are calculated, using:

$$\rho = \sum_i f_i, \quad \rho\mathbf{u} = \sum_i \mathbf{e}_i f_i \tag{16}$$

In the present paper, the multi-block lattice Boltzmann method proposed by Yu and Girimaji [22] is employed. The computational domain is divided into blocks which are connected through the interface. On the interface between blocks, the exchange of variables follows a certain relation so that the mass and momentum are conserved and the stress is continuous across the interface.

Consider a two-block system to explain the idea of the multi-block method. The ratio of lattice space between the two blocks is defined as: $m = \Delta x_c/\Delta x_f$, where Δx_c and $\Delta\ x_f$ are the lattice space of the coarse and fine mesh blocks respectively. For a given lattice space, the fluid viscosity can be obtained from Eq. (15). In order to keep a constant viscosity, the relaxation parameter τ_f in fine mesh and τ_c in coarse mesh, must

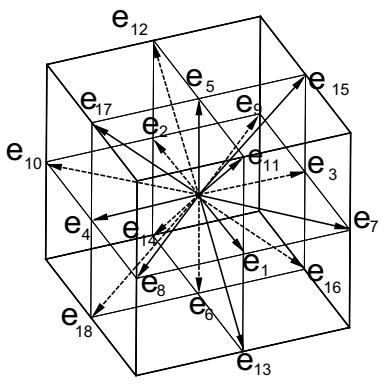

Fig. 3. D3Q19 model.

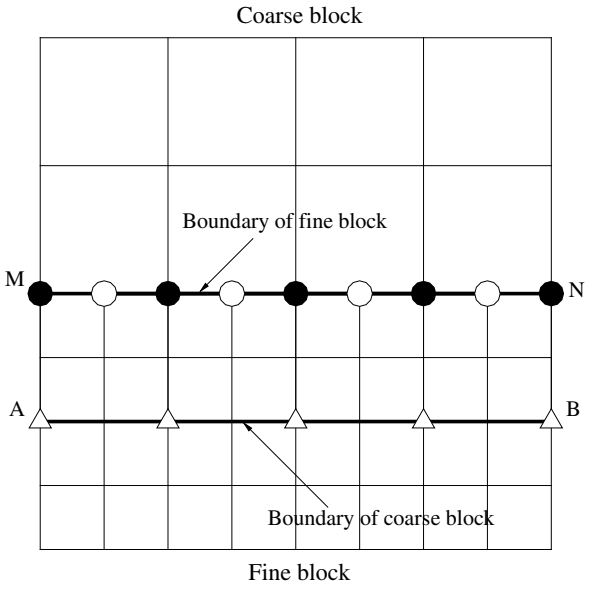

Fig. 4. Interface structures between two blocks.

satisfy the following relation: $\tau_f = 0.5 + m(\tau_c - 0.5)$. The variables and their derivatives on the grid must be continues across the block interface. To keep this continuity, the relation of the density distribution function in the neighboring blocks is proposed as

$$\tilde{f}_i^c = f_i^{eq,f} + m\frac{\tau_c - 1}{\tau_f - 1}[\tilde{f}_i^f - f_i^{eq,f}], \qquad \tilde{f}_i^f = f_i^{eq,c} + \frac{\tau_f - 1}{m(\tau_c - 1)}[\tilde{f}_i^c - f_i^{eq,c}] \tag{17}$$

where $\tilde{f}_i$ is the post-collision density distribution function.

The typical structure of interface is illustrated in Fig. 4. The fine block boundary MN is in the interior of the coarse block. The coarse block boundary AB is in the interior of the fine block. This arrangement is convenient for information exchange. Here, MN and AB represent planes projected onto the paper. On the boundary of fine block MN, there is no information on the grid points denoted by the solid symbol ● in Fig. 4. It is obtained from spatial interpolation based on the information on the grid nodes denoted by the open symbol ○ on MN. The symmetric, 2D cubic spline spatial fitting of Yu and Girimaji [22] is employed. Because the fluid particle has the same streaming velocity on each block, the computation marches m steps on the fine-mesh block for every one step on the coarse-mesh block. On the fine block boundary MN, temporal interpolation is needed to obtain $\tilde{f}_\alpha(t^{n+1/m}, \mathrm{MN})$. The three-point Lagrangian formula of Yu and Girimaji [22] is employed for temporal interpolation.

3.3. The hybrid method

In the present paper, the immersed boundary method is combined with the multi-block lattice Boltzmann method. The membrane forces of the immersed boundary method are obtained from the finite element membrane model. In order to solve the flow field with a force density the lattice Boltzmann equation must be modified. Several forms of LBE which can handle a force density have been proposed, for example the equations of He et al. [30], Luo [31] and Guo et al. [32]. Guo et al.'s approach [32] is employed here as it is accurate for unsteady flow with force changing with time and space, in which the modified lattice Boltzmann equation is in the form of:

$$f_i(\mathbf{x} + \mathbf{e}_i\Delta t, t + \Delta t) - f_i(\mathbf{x}, t) = -\frac{1}{\tau}[f_i(\mathbf{x}, t) - f_i^{eq}(\mathbf{x}, t)] + \Delta t F_i \tag{18}$$

$$\text{where } f_i^{eq} = E_i(\rho, \mathbf{u}^*) \tag{19}$$

$$\text{with } \rho\mathbf{u}^* = \sum_i \mathbf{e}_i f_i + \frac{1}{2}\mathbf{f}\Delta t \tag{20}$$

$$F_i = \left(1 - \frac{1}{2\tau}\right)\omega_i \left[\frac{\mathbf{e}_i - \mathbf{u}}{c_s^2} + \frac{(\mathbf{e}_i \cdot \mathbf{u})}{c_s^4}\mathbf{e}_i\right] \cdot \mathbf{f} \tag{21}$$

In the computation, a two-grid system is employed. The lattice space ratio between coarse and fine grids equals two. The capsules are immersed in the fine mesh block. The present procedure for multi-block computation is very similar to that proposed by Yu and Girimaji [22]. The only difference exists in the computation on the fine mesh block. That is, a subroutine implementing the immersed boundary method is added before the streaming and collision steps.

4. Results and discussion

The present method is applied to simulate the deformation of spherical, oblate spheroidal and biconcave discoid capsules in simple shear flow. The capsules are unstressed at their initial shapes. The internal and external fluids have the same property. The dimensionless shear rate is defined as: $G = \mu ka/E$, where μ is the viscosity of the surrounding fluid, k is the shear rate, E is the shear elasticity of the membrane. The equivalent radius a is defined as: $a = (3V/4\pi)^{1/3}$, where V is capsule volume. In the present study, the equivalent radius a is chosen as the length scale, ka is chosen as the velocity scale and $1/k$ the time scale. The Reynolds number defined as: $Re = \mu(ka)a/\rho$, where ρ is the density of the surrounding fluid.

4.1. Spherical capsules

4.1.1. Neo-Hookean membrane

To validate the present method, the transient deformation of spherical capsules in unbounded simple shear flow (illustrated in Fig. 5) is studied. It has been well studied by Pozrikidis [7] with ZT membrane law and Lac et al. [10] with NH membrane law. In the present section, the capsule membrane follows NH law. The Reynolds number is at 0.025.

It is important to choose a computational domain which is large enough to neglect the boundary effect and has sufficient grid resolution to obtain convergent results. Numerical simulations are carried out under various computational domain sizes and grid resolutions. The temporal evolution of the capsule's Taylor shape parameter D_{xz} is chosen as the indicator. It is defined as: $D_{xz}=(L - B)/(L + B)$, where L and B are the semimajor and semiminor lengths of the capsule in the plane of shear [10]. The dimensionless shear rate is chosen to be $G = 0.2$, at which the deformation is large.

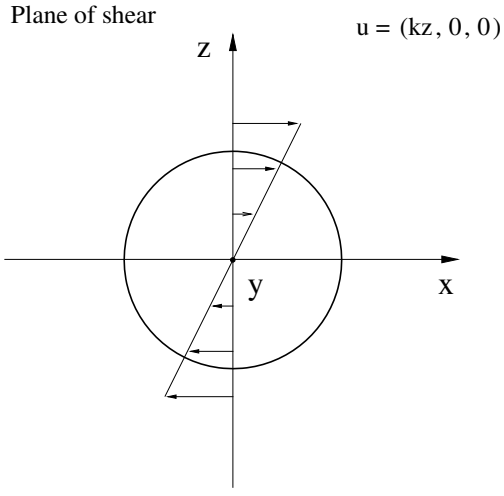

Fig. 5. Illustration of a capsule in simple shear flow.

The computational domain is a cubic box. The capsule is at the center of the domain, and its membrane is discretized into 8192 triangular elements connecting 4098 nodes. The fine mesh block covers a small cubic box, which has a side length of $4a$ and its center is coinciding with that of the computational domain. The other area is covered with coarse mesh. The grid resolutions in the fine and coarse blocks are $\Delta x_f = \Delta y_f = \Delta z_f = a/12$ and $\Delta x_c = \Delta y_c = \Delta z_c = a/6$, respectively. The computational domains with outer boundary length of $8a$, $10a$ and $12a$ are tested. The outer boundary condition is set to be the unperturbed simple shear flow. The temporal evolutions of Taylor shape parameter under various domain sizes at $G = 0.2$ are presented in Fig. 6(a). It is shown that a cubic computational domain with side $10a$ is large enough to neglect the boundary effect.

Grid convergence study is carried out on the computational domain with side $10a$. The diameter of the spherical capsule $2a$ was covered by 20, 24 or 32 lattice spaces of the fine mesh block. With the finest mesh, the capsule membrane is discretized into 32 768 flat triangular elements connecting 16 386 nodes. The temporal evolutions of Taylor shape parameter under various grid resolutions at $G = 0.2$ is presented in Fig. 6(b). From the result it is seen that the grid resolution of $\Delta x_f = \Delta y_f = \Delta z_f = a/12$, with the capsule membrane discretized into 8192 triangular elements connecting 4098 nodes, is sufficient to capture the important characteristics. This computational domain and grid resolution are used in the simulations presented in this section and Section 4.2.

Another simulation is done for the same capsule and shear rate, using uniform mesh resolution of $\Delta x_f = \Delta y_f = \Delta z_f = a/12$ covering the whole computational domain, which is actually the original IB-LBM [18,19]. It is seen that the temporal evolution of Taylor shape parameter curve (Fig. 6(b)) nearly coincide with that of the present multi-block IB-LBM. In the present method, only 6.4% of the computational domain is covered with fine mesh, thus quite a lot of computational effort is saved.

The deformation of spherical capsules with the dimensionless shear rate G ranging from 0.0125 to 0.2 is studied. The results show that after being immersed in the flow, a capsule deforms to a steady shape and inclination; then the membrane rotates around the liquid inside (tank-treading motion). These observations are similar to those reported by Pozrikidis [7] and Lac et al. [10]. For $G = 0.0125$, the steady deformed capsule and the flow field around the capsule's cross section in the plane of shear is presented in Fig. 7. It is observed that the cross section of the capsule resembles a closed streamline which shows that the capsule has achieved a steady shape. Recirculating regions are found at two ends of the capsule.

The temporal evolutions of the capsules' Taylor deformation parameter D_{xz} are presented in Fig. 8(a), and are compared with the results of Lac et al. [10] who used the boundary element method. The present model has

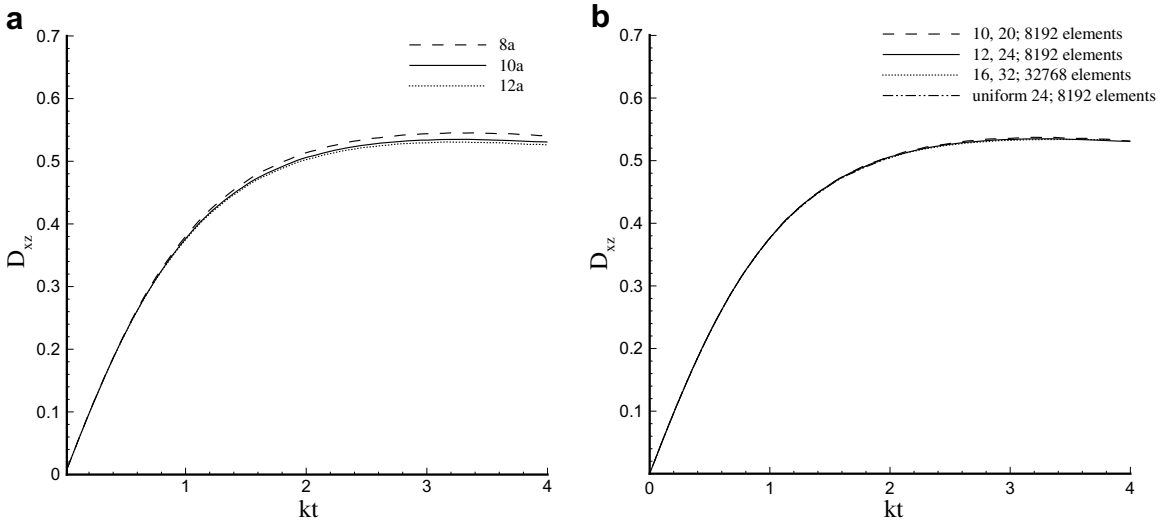

Fig. 6. Temporal evolution of the capsule's Taylor shape parameter at $G = 0.2$ under various (a) computational domain sizes; (b) grid resolutions.

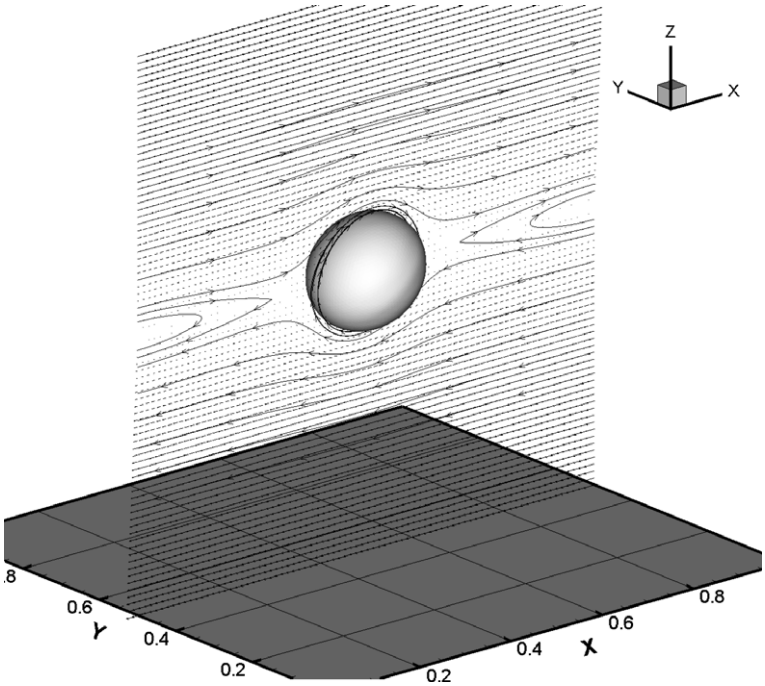

Fig. 7. Steady deformed capsule and the flow field around the cross section of the capsule in the plane of shear.

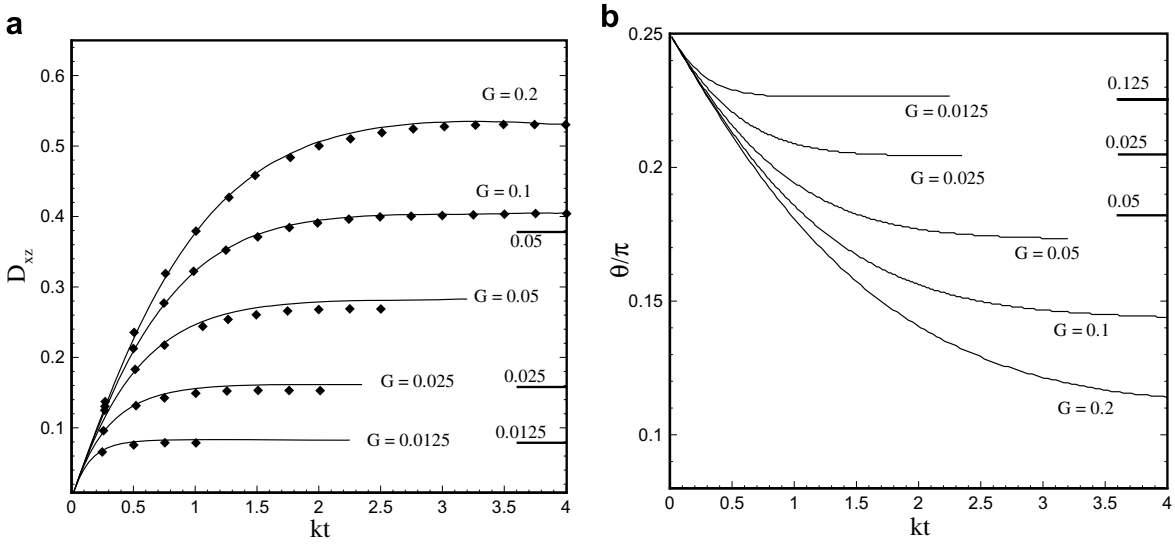

Fig. 8. Temporal evolution of (a) Taylor shape parameter; (b) inclination angle of the initially spherical capsules with NH membranes. The straight horizontal bold line represents the predictions of the second order small-deformation theory of Barthès-Biesel [1] for $G = 0.0125$, 0.025, 0.05.

considered inertia, but due to the very small Reynolds number of 0.025, the inertia effect is negligible. Good quantitative agreements are observed. It is seen the time taken to achieve steady shape is shorter if the dimensionless shear rate is lower. A lower shear rate means the ratio between elastic and shear forces is larger, thus the capsule only needs to deform a little to generate enough elastic force to balance the viscous shear force. At small dimensionless shear rates, the steady Taylor shape parameter is compared with that predicted by

Barthes-Biesel [1] who used the second order small-deformation theory. For $G = 0.0125$ and 0.025, the agreement is satisfactory (Fig. 8(a)). For $G = 0.05$, due to the relatively large deformation, the agreement is not good as the small deformation theory is not valid.

Fig. 8(b) presents the temporal evolution of the inclination angle (with respect to x-axis) of the capsule's cross section in the plane of shear. With the shear rate increasing, the capsules are observed to be more aligned with the flow. At low shear rates, the steady inclinations of the present simulation agree well with that predicted by Barthes-Biesel [1] using second order small-deformation theory.

After the capsules have achieved steady shapes, their cross sections in x–z plane are presented in Fig. 9. It is seen that at low shear rates, the capsules are slightly deformed and their cross sections are elliptical; at high shear rates, the cross sections of the deformed capsules are slender and sigmoidal.

For a spherical capsule with elastic membrane in shear flow, it will deform to a steady shape with a fixed inclination, and then the membrane rotates round the liquid inside. If the non-slip boundary condition could be strictly satisfied, the cross section of the capsule will be a perfectly closed stream line. In Fig. 10, the streamlines around the cross section of the steady deformed capsules at $G = 0.0125$ and 0.1 are presented. It is seen from Fig. 10(a) and (b) that the cross sections of the capsules seem to resemble closed streamlines. However, upon amplifying the region near the cross sections, it was found that the streamlines on the cross sections are not perfectly aligned with the capsule interface. This is more apparent at larger dimensionless shear rates when a capsule is highly deformed from a spherical shape, as shown in Fig. 10(c). However, the transverse component of the membrane velocity is much smaller than the tangential part, so that the capsule could still tank tread with a nearly steady shape for a very long time. In a recent paper, Lallemand et al. [20] proposed the front tracking lattice Boltzmann method in which the non-slip boundary condition can be accurately achieved.

4.1.2. Skalak membrane

As another validation of the present method, the transient deformation of spherical capsules with Skalak membrane in unbounded shear flow is studied. The moduli ratio C in Eq. (3) is chosen to be 1 to be the same as that of Lac et al. [10] who used the BEM. The Reynolds number in the present study equals 0.025. The computational domain and grid resolution are the same as that in the last section.

Similar with the results of previous Section 4.1.1, the capsule deforms to a steady shape and then the membrane carries out tank-treading motion. The temporal evolutions of the capsules' Taylor deformation parameter are presented in Fig. 11(a). The steady values are compared with the previous results reported by Lac et al. [10] using boundary element method. Satisfactory agreements are observed with the results of Lac et al. whose capillary number ε is related to the dimensionless shear rate G of the present study by: $\varepsilon = 2G$. Fig. 11(b) presents the temporal evolution of the inclination angle of the capsule's cross section of in the plane of shear. However there is no previous result with SK membrane available for comparison. It is seen that with the shear rate increasing, the capsules are more aligned with the flow.

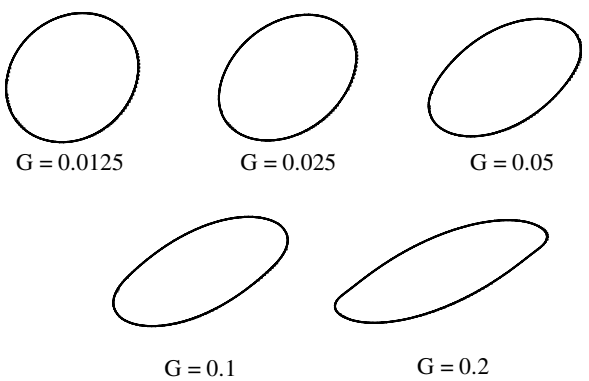

Fig. 9. Cross sections of the steady formed capsules in the plane of shear.

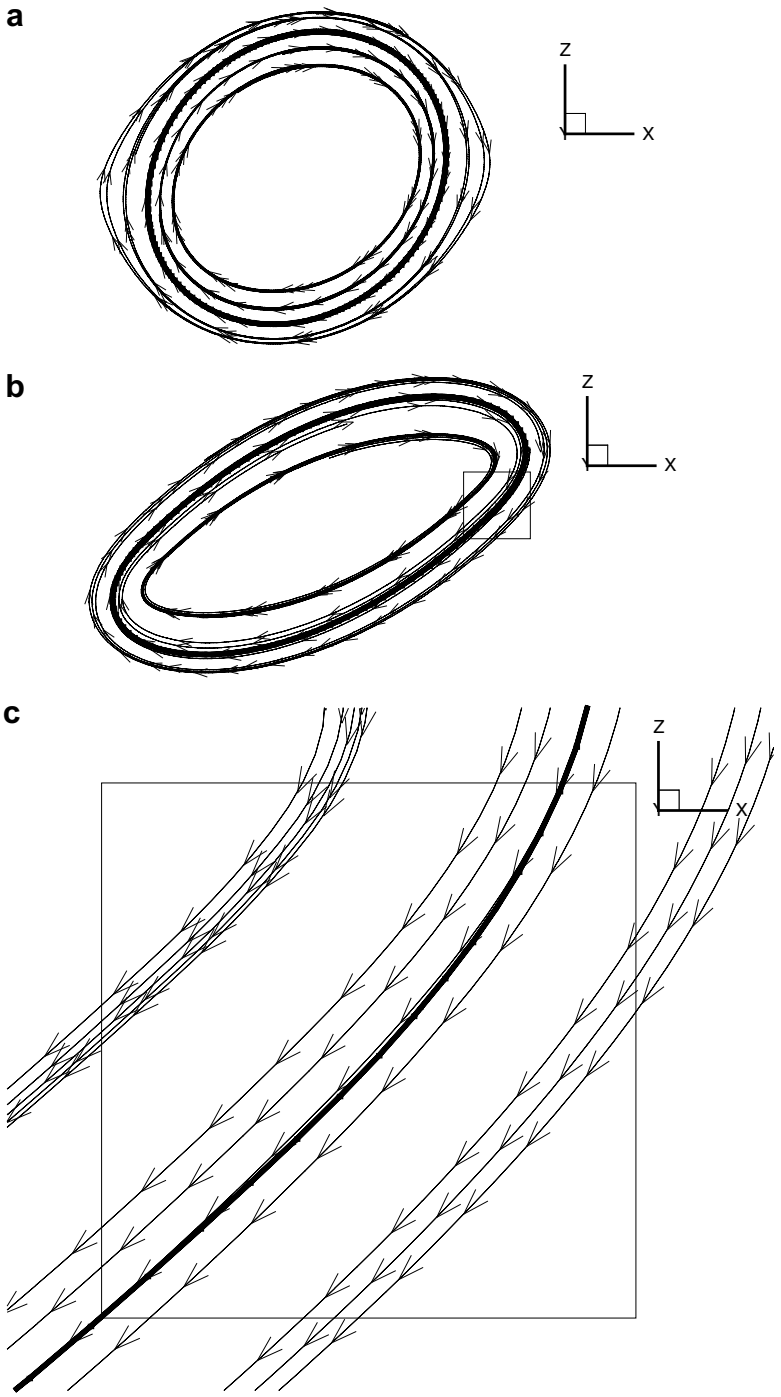

Fig. 10. Streamlines around the cross sections of the steady formed capsules in the plane of shear (a) $G = 0.0125$; (b) $G = 0.1$; (c) regional amplification for (b). The bold solid lines represent the membrane.

4.2. Oblate spheroidal capsules

As a further validation of the present method, the transient deformation of oblate spheriodal capsules, with semimajor to semiminor axes ratio of 10:9 and 2:1, in shear flow is studied. These cases are more challenging

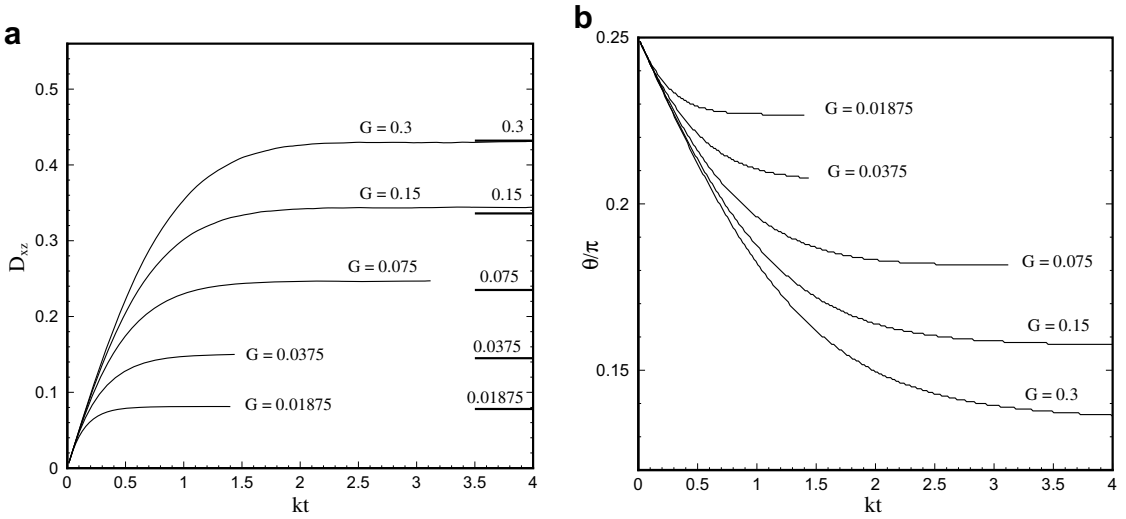

Fig. 11. Temporal evolution of (a) Taylor shape parameter; (b) inclination angle of the initially spherical capsules with SK membranes. The straight horizontal bold line represents results of Lac et al. [10].

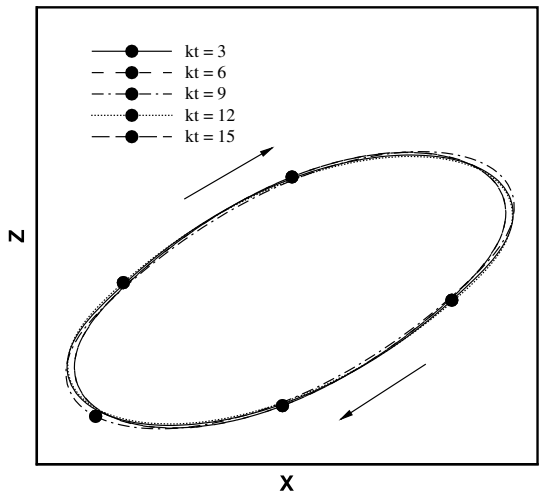

Fig. 12. Snapshots of an initially oblate spheroidal capsule's cross section in the plane of shear during the tank treading motion. The symbol ● represents the same membrane node which is moving.

than those in the previous section because of the more complicated capsule shapes. In this section, the capsules membrane follows zero-thickness law, same as that of Ramanujan and Pozrikidis [8] who used BEM. The Reynolds number in the present study is at 0.025. The computational domain and grid resolution is this section is the same as that in the previous sections.

For a spherical capsule in shear flow, the capsule deforms and then the membrane performs tank treading around the liquid inside. During this tank treading motion, the shape and inclination of the capsule remains unchanged. The motion of oblate spheroidal capsules is different. It has been observed that after a transient stage, the capsule membrane rotates around the liquid inside; during this tank treading motion, the capsule undergoes periodical shape deformation and inclination oscillation. The results are similar to those predicted by Ramanujan and Pozrikidis [8] For a capsule with semimajor to semiminor axes ratio of 10:9 at $G = 0.1$, the snapshots of the capsule's cross section in the plane of shear during the unsteady tank treading motion are presented in Fig. 12. It is seen that the capsule are changing shape and inclination while its membrane is rotating round the liquid inside.

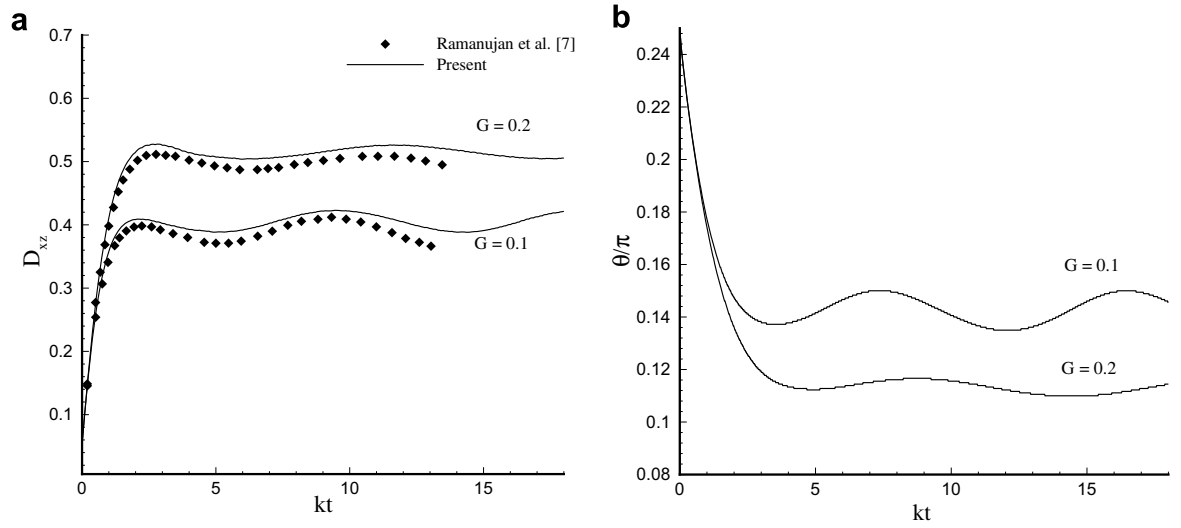

Fig. 13. Temporal evolution of (a) Taylor shape parameter; (b) inclination angle of oblate spheroidal capsules with semimajor to semiminor axes ratio of 10:9.

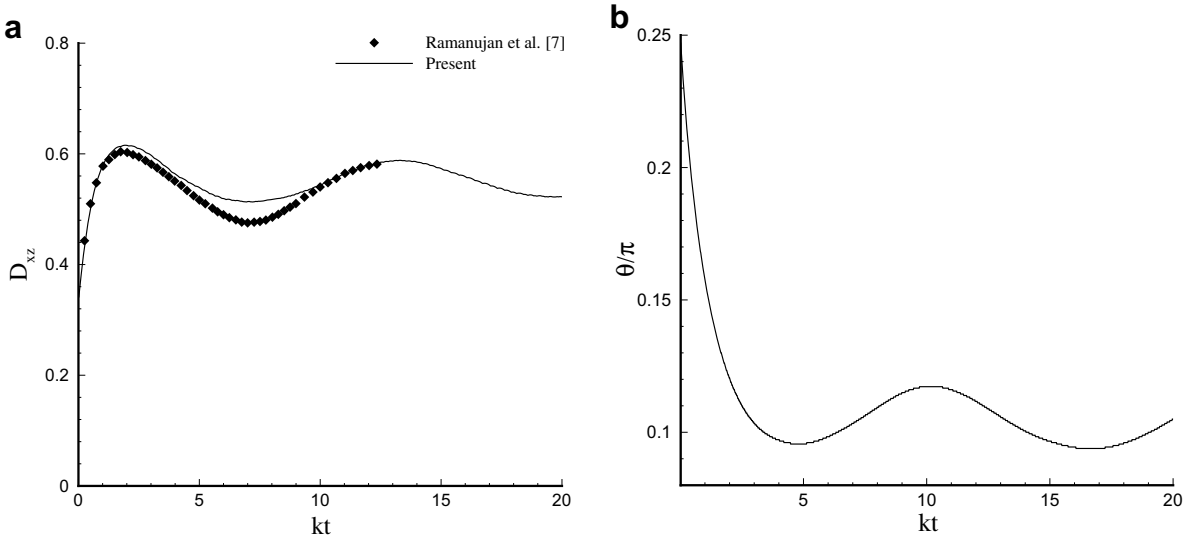

Fig. 14. Temporal evolution of (a) Taylor shape parameter; (b) inclination angle of oblate spheroidal capsules with semimajor to semiminor axes ratio of 2:1.

The temporal evolutions of the capsules' Taylor deformation parameter and inclination angle are presented in Fig. 13(a) and (b) for capsules with semimajor to semiminor axes ratio of 10:9 at $G = 0.1$ and 0.2. The results of a more oblate capsule is presented in Fig. 14(a) and (b), which are for capsules with semimajor to semiminor axes ratio of 2:1 at $G = 0.2$. The results of Ramanujan and Pozrikidis [8] are also presented in Figs. 13 and 14(a). Satisfactory agreements are observed.

4.3. Inertia effects

To demonstrate the versatility of the present method, the effect of inertia is considered. The linear shear flow past spherical capsules with neo-Hookean membranes is studied at Reynolds number ranging from

0.25 to 25. To our knowledge, the effect of inertia on the transient deformation of three-dimensional liquid-filled capsules with elastic membranes has not been explored so far.

The linear shear flow is generated by two solid walls moving in opposite directions. The computational domain is a cubic box with length $8a$, which is the distance between the two moving walls. The capsule is at the center of the domain. The boundary conditions at the upper and lower planes of the computational domain are set as solid walls moving in opposite directions. Periodic boundary conditions are employed on the other four boundary planes. For $Re = 0.25$ and 2.5, the fine mesh block covers from $2a$ to $6a$ in all axes. The grid resolutions in coarse and fine blocks and the disretization of the membrane are the same as those in the previous sections. For $Re = 10$ and 25, the fine mesh block covers from $1.5a$ to $6.5a$ in all axes, and the grid resolutions are: $\Delta x_c = \Delta y_c = \Delta z_c = a/8$, $\Delta x_f = \Delta y_f = \Delta z_f = a/16$. The membrane is discretized into 32 768 flat triangular elements connecting 16 386 nodes. Grid convergence studies showed that the mesh resolutions are sufficient.

The temporal evolutions of the capsules' Taylor shape parameter and inclination angle are presented in Fig. 15(a) and (b) for $G = 0.05$ and in Fig. 16(a) and (b) for $G = 0.1$, with Reynolds number ranging from 0.025 to 25. At moderate Reynolds numbers, it is quite interesting to find that before the capsules achieve steady states, there is a transient process due to the inertia effect, especially apparent at higher Reynolds numbers. This phenomenon is quite different from that of capsule deformation in simple shear flow at vanishing Reynolds number, in which the capsules achieve steady states monotonically. In the transient period, the Taylor shape parameter and capsule inclination show dampened oscillations. Similar transient process, which is due to the effect of inertia, has been observed for liquid drops in the numerical study of Lee and Pozrikidis [33].

After the transient period, the capsules achieve steady configurations. Through comparison of the steady Taylor shape parameters at different Reynolds numbers, it is found that the inertia effect promotes the capsule deformation. It is also found that the curves for $Re = 0.25$ are comparable with that for $Re = 0.025$, which may suggest that the inertia effect on the capsule deformation is still very small up to $Re = 0.25$.

Inertia effect tends to increase the capsule deformation; it also induces an initial transient process, in which the capsule's shape and inclination show dampened oscillations at larger Reynolds number. Thus for a capsule under the same shear rate, the time it takes to achieve a steady state is longer at higher Reynolds number. In Figs. 15 and 16 the computations were stopped shortly after steady state was achieved.

For all cases considered, the capsule achieves a steady state. The flow fields in the plane of shear around the cross sections of the capsules for $G = 0.1$ are plotted in Fig. 17 for different Reynolds number from 0.25 to 25.

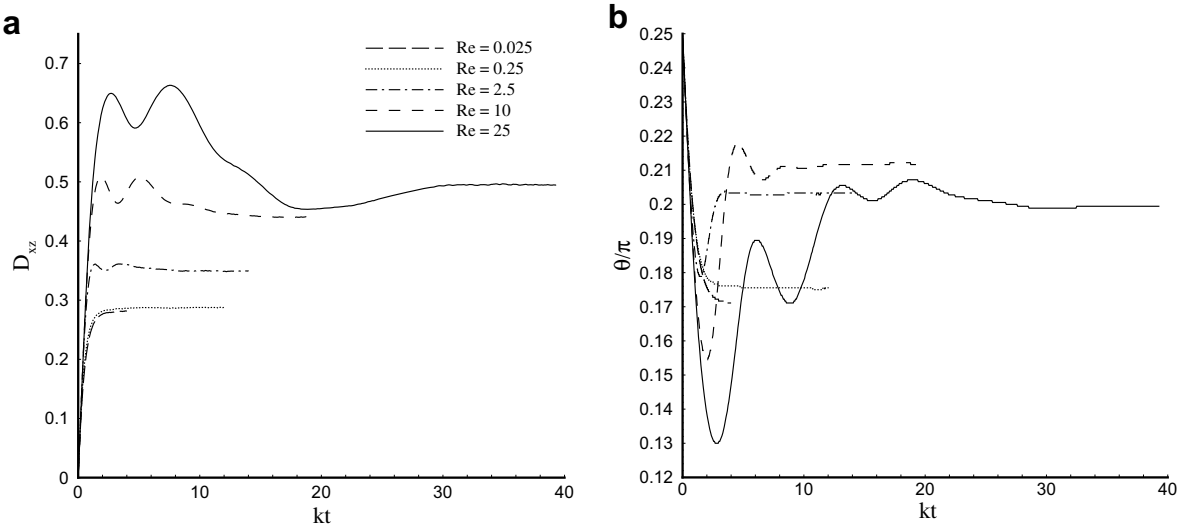

Fig. 15. Temporal evolution of (a) Taylor shape parameter; (b) inclination angle of spherical capsules with NH membrane at $G = 0.05$ under various Reynolds numbers.

It is seen that the cross sections of the capsules, which are represented by bold solid lines, resemble closed streamlines. This shows that the capsules have achieved steady shapes. Through comparison of the flow field, it is found that inertia has significant effect. For example, the size of recirculating regions increases with the Reynolds number increasing.

It is also interesting to investigate steady three-dimensional configuration of the capsules at various Reynolds numbers. Fig. 18(a) and (b) present the steady profiles of capsules at $Re = 0.25$ and 25 at dimensionless shear rate $G = 0.1$. The corresponding cross-sections of the capsules can be found in the previous Fig. 17(a) and (d). At small $Re = 0.25$, the capsule achieves an ellipsoidal shape. However at moderate $Re = 25$, the

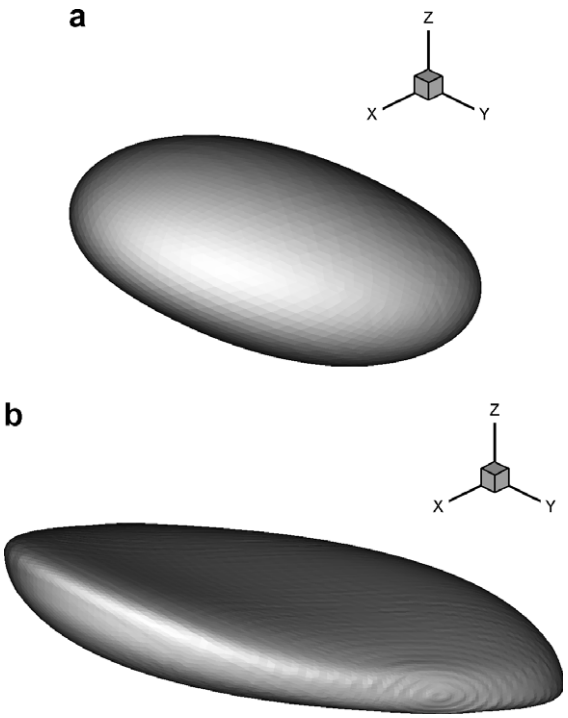

Fig. 18. Steady profiles of the capsules at (a) $Re = 0.25$; (b) $Re = 25$.

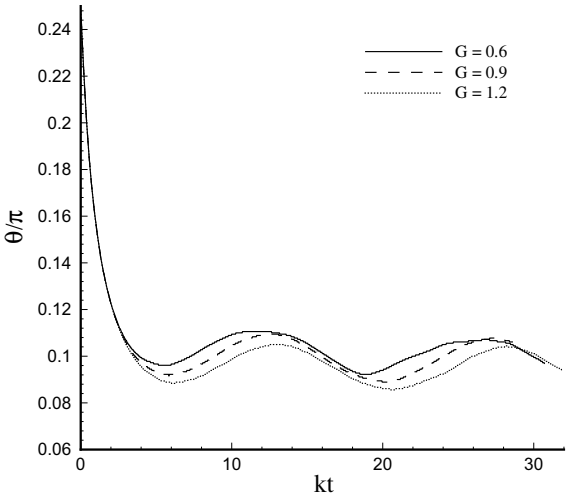

Fig. 19. Temporal evolution of the inclination angle of the initially biconcave capsule.

steady shape looks very different. It resembles a flat disk, with two ends of large curvature pointing upwards or downwards.

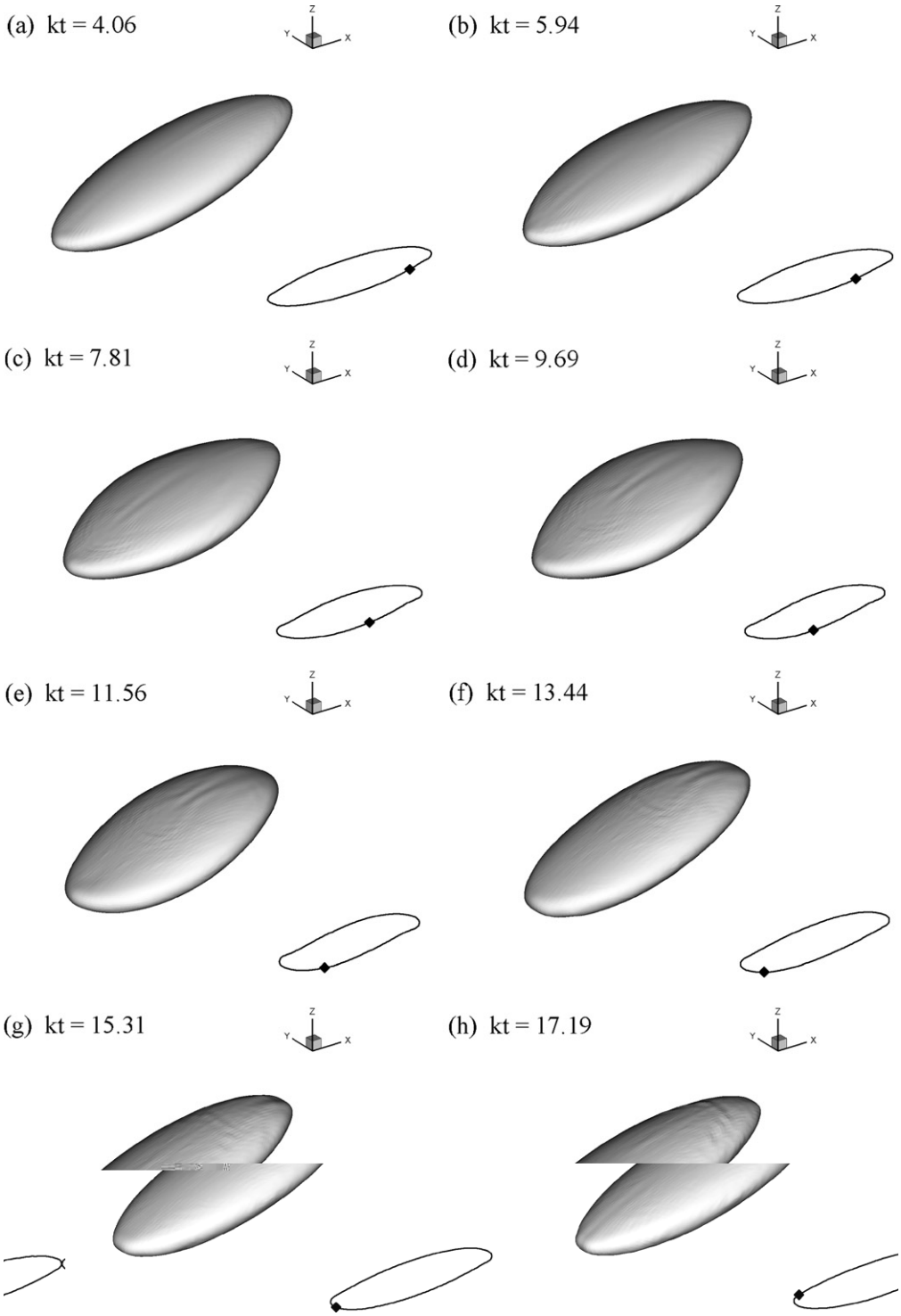

Fig. 20. Snapshots of the capsule during the tank-treading motion. The diamond symbol represents the same membrane node on the capsule's cross section, which is moving in the plane of shear.

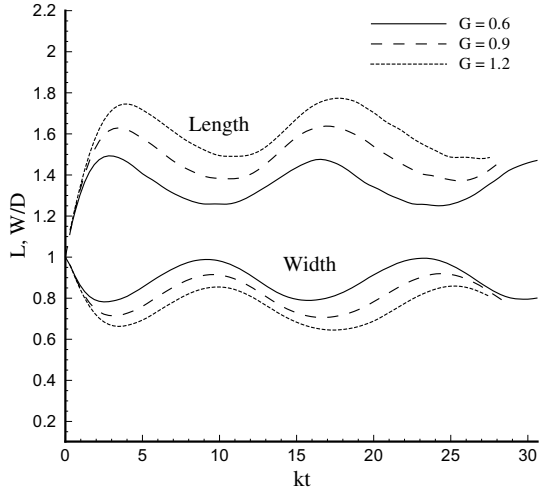

Fig. 21. Temporal evolution of the capsule's length and width. D is the initial diameter of the biconcave disk.

4.4. Biconcave capsules

For biconcave capsules, whose shape resembles that of red blood cells, it is expected that they will carry out tank treading motion in simple shear flow if the internal liquid is same as that outside and the shear rate is large [8]. However, due to the complex geometry of the capsule, numerical instabilities were encountered in previous computations, and the behavior was followed for an initial short stage [8,9]. So far, the tank treading motion for three-dimensional biconcave capsules has not been fully recovered by numerical simulation.

To demonstrate the capacity of the present method, the deformation of capsules with biconcave shape is studied in simple shear flow in this section. The membrane of the capsule follows Skalak's law (Eq. (3)), in which the moduli ratio C is chosen to be 200 to take the membrane incompressibility into account. The computational domain is a cubic box with side length $10a$. The fine mesh block covers from $2a$ to $8a$ in all axes, and the grid resolutions are: $\Delta x_f = \Delta y_f = \Delta z_f = a/8$, $\Delta x_f = \Delta y_f = \Delta z_f = a/16$. The membrane is discretized into 32 768 flat triangular elements connecting 16 386 nodes, which is sufficient to capture the important characteristics.

Simulations are carried out for the deformation of capsules at $G = 0.6$, 0.9 and 1.2, with $Re = 0.25$. The tank treading motion (the membrane rotates around the liquid inside) is observed. Similar to that of oblate spheroidal capsules, during this tank treading motion, the capsule undergoes periodical shape deformation and inclination oscillation. This unsteady tank-treading motion had been expected by Ramanujan and Pozrikidis [8] in their study in which the motion was followed for an initial short stage.

The temporal evolution of the capsules' inclination angle is presented in Fig. 19. To illustrate the capsules' shape evolution during this unsteady tank-treading motion, the snapshots of the capsule' profiles at $G = 0.9$ are presently in Fig. 20 at sequential dimensionless times. The legends at the lower right of the figures represent the cross sections of the capsule in the plane of shear. The diamond symbol represents the same membrane node. It is seen from Fig. 20 that during the membrane rotating around the liquid inside, the capsule is changing its shape and inclination. It is interesting to find that when the capsule is most elongated, its width (in y direction) is smallest, and vice visa. This phenomenon can also be observed from Fig. 21, in which the temporal evolution of the capsule's length and width is presented. The simulation is stopped after the capsule membrane has been rotating for a whole period. For all cases in this section, the membrane area change is within 1% and the capsule volume change is within 0.2% during the computation.

5. Conclusions

A hybrid method is proposed to study the flow-induced deformation of three-dimensional, liquid-filled capsules with elastic membranes. In the present approach, the immersed boundary concept is incorporated into

the lattice Boltzmann method; and the multi-block strategy is employed to refine the mesh near the capsule. A finite element model is incorporated to obtain the forces acting on the membrane nodes of the three-dimensional capsule which is discretized into flat triangular elements. The present method was validated by studying the transient deformation of initially spherical and oblate spheroidal capsules with various membrane laws under shear flow. The present results agree well with published theoretical or numerical results. Compared with the original immersed boundary-lattice Boltzmann method using uniform mesh in the whole computational domain [18,19], the present method is much more efficient. The present method is capable to take the inertia effect into account. This was demonstrated by studying the deformation of spherical capsules in shear flow at moderate Reynolds numbers, which has not be investigated so far. It was found that inertia has significant effects on the transient deforming process and steady configurations of capsules, as well as on the flow field. The transient deformation of capsules with initially biconcave disk shape was also simulated. The unsteady tank treading motion was followed for a whole period in the present work. Due to numerical instabilities encountered in previous computations [8,9], this motion has not been recovered by numerical simulation so far.

References

[1] D. Barthès-Biesel, Motion of spherical microcapsule freely suspended in a linear shear flow, J. Fluid Mech. 100 (1980) 831–853.
[2] D. Barthès-Biesel, J.M. Rallison, The time-dependent deformation of a capsule freely suspended in a linear shear flow, J. Fluid Mech. 113 (1981) 251–267.
[3] C.W. Hirt, A.A. Amsden, J.L. Cook, An arbitrary Lagrangian–Eulerian computing method for all flow speeds, J. Comput. Phys. 14 (1974) 227–253.
[4] H. Liu, K. Kawachi, A numerical study of undulatory swimming, J. Comput. Phys. 155 (1999) 223–247.
[5] T. Biben, C. Misbah, Tumbling of vesicles under shear flow within an advected-field approach, Phys. Rev. E 67 (2003) 031908.
[6] C. Pozrikidis, Boundary Integral and Singularity Methods for Linearized Viscous Flow, Cambridge University Press, 1992.
[7] C. Pozrikidis, Finite deformation of liquid capsules enclosed by elastic membranes in simple shear flow, J. Fluid Mech. 297 (1995) 123–152.
[8] S. Ramanujan, C. Pozrikidis, Deformation of liquid capsules enclosed by elastic membranes in simple shear flow: large deformations and the effect of capsule viscosity, J. Fluid Mech. 361 (1998) 117–143.
[9] C. Pozrikidis, Numerical simulation of the flow-induced deformation of red blood cells, Annals Biomed. Eng. 31 (2003) 1194–1205.
[10] E. Lac, D. Barthes-Biesel, N.A. Pelekasis, J. Tsamopoulos, Spherical capsules in three-dimensional unbounded Stokes flows: effect of the membrane constitutive law and onset of buckling, J. Fluid Mech. 516 (2004) 303–334.
[11] C.S. Peskin, Numerical analysis of blood flow in the heart, J. Comput. Phys. 25 (1977) 220–252.
[12] C.S. Peskin, The immersed boundary method, Acta Numer. 11 (2002) 479–517.
[13] C.D. Eggleton, A.S. Popel, Large deformation of red blood cell ghosts in s simple shear flow 10 (8) (1998) 1834–1845.
[14] S. Chen, G.D. Doolen, Lattice Boltzmann method for fluid flows, Ann. Rev. Fluid Mech. 30 (1998) 329–364.
[15] D. Yu, R. Mei, L. Luo, W. Shyy, Viscous flow computations with the method of lattice Boltzmann equation, Prog. Aerospace Sci. 39 (2003) 329–367.
[16] A.J.C. Ladd, Numerical simulations of particulate suspensions via a discretized Boltzmann equation Part I. Theoretical foundation, J. Fluid. Mech. 271 (1994) 285–310.
[17] A.J.C. Ladd, Numerical simulations of particulate suspensions via a discretized Boltzmann equation. Part II. Numerical results, J. Fluid Mech. 271 (1994) 311–339.
[18] Z.G. Feng, E.E. Michaelides, The immersed boundary-lattice boltzmann method for solving fluid–particles interaction problems, J. Comput. Phys. 195 (2004) 602–628.
[19] Z.G. Feng, E.E. Michaelides, Proteus: a direct forcing method in the simulations of particulate flows, J. Comput. Phys. 202 (2005) 20–51.
[20] P. Lallemand, L.-S. Luo, Y. Peng, A lattice Boltzmann front-track method for interface dynamics with surface tension in two-dimensions, J. Comput. Phys. 226 (2007) 1367–1384.
[21] O. Filippova, D. Hänel, Grid refinement for lattice-BGK models, J. Comput. Phys. 147 (1998) 219–228.
[22] D. Yu, S.S. Girimaji, Multi-block lattice Boltzmann method: extension to 3D and validation in turbulence, Physica A 362 (2006) 118–124.
[23] Y. Peng, C. Shu, Y.T. Chew, X.D. Niu, X.Y. Lu, Application of multi-block approach in the immersed boundary-lattice Boltzmann method for viscous fluid flows, J. Comput. Phys. 218 (2006) 460–478.
[24] Y. Sui, Y.T. Chew, P. Roy, H.T. Low, A hybrid immersed-boundary and multi-block lattice Boltzmann method for simulating fluid and moving-boundaries interactions, Int. J. Numer. Methods Fluids 53 (2007) 1727–1754.
[25] Y. Sui, Y.T. Chew, P. Roy, X.B. Chen, H.T. Low, Transient deformation of elastic capsules in shear flow: effect of membrane bending stiffness, Phys. Rev. E 75 (2007) 066301.
[26] J.M. Charrier, S. Shrivastava, R. Wu, Free and constrained inflation of elastic membranes in relation to thermoforming non-axisymmetric problems, J. Strain Anal. 24 (1989) 55–74.

[27] S. Shrivastava, J. Tang, Large deformation finite element analysis of non-linear viscoelastic membranes with reference to thermoforming, J. Strain Anal. 28 (1993) 31–51.
[28] R. Skalak, A. Tozeren, R.P. Zarda, S. Chien, Strain energy function of red blood cell membranes, Biophys. J. 13 (1973) 245–264.
[29] P.L. Bhatnagar, E.P. Gross, M. Krook, A model for collision processes in gases. I. Small amplitude processes in charged and neutral one-component systems, Phys. Rev. 94 (1954) 511–525.
[30] X. He, Q. Zou, L.-S. Luo, M. Dembo, Analytic solutions and analysis on non-slip boundary condition for the lattice Boltzmann BGK model, J. Stat. Phys. 87 (1997) 115–136.
[31] L.-S. Luo, Theory of the lattice Boltzmann method: Lattice Boltzmann models for nonideal gases, Phys. Rev. E 62 (2000) 4982–4996.
[32] Z.L. Guo, C.G. Zheng, B.C. Shi, Discrete lattice effects on the forcing term in the lattice Boltzmann method, Phys. Rev. E 65 (2002) 046308.
[33] J. Lee, C. Pozrikidis, Effect of surfactants on the deformation of drops and bubbles in Navier–Stokes flow, Comput. Fluids 35 (2006) 43–60.